metals

MDPI

Article

Molecular Dynamics Study of Temperature Dependence of Grain Boundaries (100) in Pure Aluminum with Application of Machine Learning

Evgenii V. Fomin

Department of General and Theoretical Physics, Chelyabinsk State University, 454001 Chelyabinsk, Russia; fomin33312@gmail.com

Abstract: As is known, grain boundary (GB) energy determines the mobility of GBs and their population in metals. In this work, we study the energy of GBs in the (100) crystallographic plane and in the temperature range from 100 to 700 K. The study is carried out using both the molecular dynamic (MD) method and machine learning approach to approximate the MD data in order to obtain functional dependence in the form of a feed-forward neural network (FCNN). We consider the tilt and twist grain boundaries in the range of misorientation angles from 0 to 90°. Also, we calculate the average and minimum energy over the ensemble of GB states, since there are many stable and metastable structures with different energies even at a fixed grain misorientation. The minimum energies decrease with increasing temperature, which is consistent with the results of other studies. The scatter of GB energies in the temperature range from 100 to 700 K is obtained on the basis of MD simulation data. The obtained energy spread is in reasonable agreement with the data from other works on the values of GB energy in pure aluminum. The predictive ability of the trained FCNN as well as its ability to interpolate between the energy and temperature points from MD data are both demonstrated.

Keywords: grain boundaries; grain boundary energy; temperature dependence; machine learning; artificial neural networks

check for updates

Citation: Fomin, E.V. Molecular Dynamics Study of Temperature Dependence of Grain Boundaries (100) in Pure Aluminum with Application of Machine Learning. *Metals* **2024**, *14*, 415. https://doi.org/10.3390/met14040415

Academic Editors: João Manuel R. S. Tavares and José Machado

Received: 23 February 2024
Revised: 26 March 2024
Accepted: 29 March 2024
Published: 31 March 2024

1. Introduction

The study of grain boundaries (GBs) in metals and alloys is currently at the center of attention of researchers, despite the fact that GBs have been actively studied in various materials for several decades using experimental and numerical methods. This is due to the fact that the distribution and structure of GBs have a significant influence on the mechanical and strength properties of materials. GB mobility leads to the occurrence of recrystallisation and grain growth processes and corresponding changes in the overall microstructure of the material [1–3]. Grain boundaries can be sources of crystal structure defects such as dislocations [4–7], and GBs are also able to interact with mobile dislocations from crystal grains [8]. In addition, GBs can be initiators of cracks, the propagation of which leads to the subsequent fracture of materials [9,10]. At the same time, GBs affect the strength and mechanical properties of metals and alloys of various types, whether they are samples with FCC [10] or BCC [11] lattices or more complex materials, namely high-entropy alloys, where the lattice type may depend on the concentration of certain alloy elements [9]. The GBs are generally determined through 5 degrees of freedom: Three are related to grain misorientation, and two determine the boundary plane. In most cases, other physical values are used to indicate and classify GBs. For example, the overwhelming number of articles use the value Σ: The inverse density of coincidences of atoms at the boundary plane. The boundaries with small values Σ and small excess energies are called "special", while the boundaries with other values of Σ are called "general". Often, the study of GBs is limited to only some cases when the boundary plane is fixed, and the misorientation is set

by rotating or twisting the grains around some crystallographic plane, for example, (100), (110), or (111). In this case, the concept of tilt and twist boundaries is introduced, and often in such types of GBs, the concepts of low-angle (misorientation angle less than 15°) and high-angle (misorientation angle greater than or equal to 15°) are used.

In turn, the GBs energy determines some important properties: Mobility of the GBs both under annealing conditions [1,12] and under the action of high stress and temperature, for example, in cutting processes [3]. The GB energy also determines the distribution of grain boundaries and the population of different types of boundaries in polycrystals [13,14]. Early studies of GBs energy were based mainly on experimental data, analysis of grain geometry [15,16], and numerical studies based on atomistic modelling techniques [16]. These works contain a rather small number of investigated boundaries due to the difficulty of their measurement in the case of experiments and the insufficient computing resources available at that time in the case of numerical studies. In the second case, the accuracy of the interatomic potentials must also be taken into account. All this led to the fact that the results obtained in these works give a good qualitative and some quantitative insight into the GB energy distribution in symmetric tilt and twist grain boundaries. However, these results needed to be refined by studying different types of GBs. The historical development of numerical modelling methods, namely classical molecular dynamics (MD) and *ab initio* methods, has led to the appearance of a large amount of data on the energy of different GB types. Over time, some quantitative discrepancy between the experimental energies of GBs and the obtained energies from atomistic simulations has been noted, as can be seen in the example of symmetric tilt boundaries in copper [17]. In [18], the authors investigated the distribution of GB population from the energy of boundaries in austenitic steel based on experimental data and atomistic modelling results. The measured energies differed in some cases, for example, for the coherent twin boundary Σ3, but the values of the GB population indicate that the measurement of MD calculations are more correct. The authors attribute this to the insufficient amount of experimental measurement variation that can be obtained. One can trace the influence of the development of atomistic modelling methods on the study of the energy of GBs in the following works, in which the authors developed a technique for creating large datasets of GBs of different configurations [19], or studies related to the measurement of the energy of a large number of special GBs with sufficient accuracy for different metals: FCC metals [5,6,14,20–23] or BCC metals [18,23,24]. As noted earlier, the use of the MD method allows for the creation of large datasets with GB energy of different types and misorientations, which allowed the formulation of fully anisotropic interpolation functions of GB energy by Bulatov, Reed, and Kumar (BRK function) for FCC metals [25] and their extension for BCC metals using iron as an example by other authors [24]. The growth of computing resources and the development of first-principles methods have led to a number of works where GB energies are systematically investigated by *ab initio* calculations. In these works, the authors study many different materials (FCC, BCC and HPC lattice metals) and propose universal GB energy functions in the form of a linear regression [26] or a decision tree trained by the random forest method [27].

In the last 5–10 years, machine learning methods have been applied to the study of GBs. For example, in [28], a trained SVM regression model that can predict both the structure of special boundaries and their energies with sufficient accuracy is shown on data from molecular statistic (MS) modelling of optimal structures of symmetric tilt GBs in pure copper. The use of machine learning methods can also be indirect: In atomistic modelling using NNP interatomic potentials. In [29], the obtained energies of symmetric tilt and twist GBs for six FCC metals are obtained from MD calculations with NNP potentials, and it is shown that the obtained GB energies are in good agreement with density functional theory (DFT) calculations, which is especially important when classical interatomic potentials give rather large errors in the GB energies. Also, machine learning methods are used to study the segregation of dissolved atoms in the alloy at the GBs, which is an important problem since the deposition of atoms at the boundary can have a strong influence on the mechanical and strength properties. In [30], the use of the extremely randomized tree

classifier method is shown to solve this problem. This method classifies MD simulation data of the dissolution of Co, Fe, Mg, Ni, Pb, and Ti atoms in the aluminum-based polycrystal and relates GB symmetry to atomic solubility. The work [31] shows that the use of decision tree regression is allowed to more accurately describe the process of atom segregation at the GBs in comparison with analytical theories, since the machine learning model takes into account the GB structure and the different segregation energies.

The practical significance of studying the energy of GBs of different types is justified by the fact that such physical processes as recrystallisation and the evolution of grain structure in polycrystals in the process of annealing or under the action of load depend on the mobility of GBs, which depends on the GB energy. Experimental studies of GB motion in Al_2O_3 at the atomic level [32] show that the boundary structure changes inhomogeneously during its motion. The authors show that the GB motion gives rise to grain boundary structural units that change depending on the local curvature of the boundary, and these structural units have different energies [22]. In recent works, it has been shown that the use of anisotropic BRK energy functions compared to isotropic energy functions of GBs gives qualitatively and quantitatively different results for the processes of grain growth, the motion of triple junctions [2], and the process of grain structure evolution in general. The use of the BRK energy function for modelling microstructure evolution by the voxel method leads to the fact that the GB distribution is shifted to low-energy boundaries [12]. Modelling of microstructure evolution taking into account the boundary energy anisotropy in MgO crystal by the phase field method also shows a high density of GBs with small values of Σ, which correlates with the experimental data [1]. It is possible to account for the anisotropy of the GB energy not only by continuous dependencies such as the Reed–Shockley or the BRK functions but even as a database. In [33], it is shown that phase field modelling with the inclusion of the GB energy database leads to slower polycrystal boundary kinetics, in contrast to modelling using an isotopic GB energy function. Also, the authors of [33] demonstrate the appearance of a larger number of low-angle boundaries.

In many works, the energy and structure of GBs are investigated for stable structures with minimum energy using molecular statics [20–22,28] or dynamics methods at very low temperatures, e.g., 10 K [5,34]. Existing approximation functions of the boundary energy, such as the BRK function, are based on these data [24,25]. In the general case, GBs can exist not only in stable but also in metastable states, which gives a rather strong scatter in energy and structure even for the boundary with fixed misorientation. This is shown in [23] in the example of symmetric tilt and twist GBs in aluminum, silicon, and tungsten. The authors [6] consider GBs with fixed misorientation of the boundary and show that for the tilt GB Σ5 in the plane (110) there are 1 stable and 15 metastable structures, and the energy differences range from 465 to 654 mJ/m^2. These structures are observed both for the molecular static case (T = 0 K) and at the system temperature (T = 300 K). In further studies [35], the authors showed that the structural stability of metastable GB structures can depend on temperature, and an interesting phenomenon in terms of the strength properties of materials is observed: the yield strength for metastable boundaries can be higher than for stable structures.

In addition to the features of the GB structure, temperature is a significant factor affecting the grain boundary energy in pure metals. This is confirmed by experimental data: In [36], a decrease in the relative GB energy in Al_2O_3 with increasing temperature from 1450 to 1650 K is observed. The decrease in the boundary energy with increasing temperature is also observed for symmetric tilt GBs in FCC metals [22], which is shown by the authors on the example of boundaries Σ7, Σ13b, Σ49, Σ19b, Σ37c. The energy of the structural units of these boundaries decreases with increasing temperature. The total energy of GB also decreases with increasing temperature, as shown by the special boundary Σ79 in nickel [37]. Just as accounting for the anisotropy of the GB energy provides a more detailed description of the boundary motion and changes in the microstructures of polycrystals, accounting for the GB energy as a function of temperature also contributes to the description of the

boundary motion. For example, to explain anomalous grain growth at certain temperatures, was which discussed in [36].

Summarizing the above, it can be concluded that the study of temperature dependence is relevant at the present, since there are no scientific works systematically investigating the effect of temperature on a wide range of grain boundaries. In this paper, the GB energies of different types (tilt and twist) in the (100) crystallographic plane for pure aluminum are investigated. The energies for temperatures 100, 300, 500, and 700 K are calculated on the basis of MD simulations of maintaining bicrystalline samples with different grain misorientations at a constant temperature. The temperature dependences of the GB energy obtained at the stage of MD simulations of maintaining bicrystals at constant temperature are shown. The scattering diagram of GB energies in the temperature range from 100 to 700 K is constructed. The final part of the work is devoted to the description of the function of GB energy from grain misorientation and temperature in the form of a fully connected feed-forward neural network (FCNN). Correlation curves on training, validation, and test datasets are constructed, and the results of two variants of FCNN, with piecewise linear and non-linear activation functions in hidden layers with energy values from MD calculations are compared. Based on the trained FCNN with non-linear activation functions, energy plots at intermediate temperatures are not contained in the datasets.

2. Materials and Methods

In this work, aluminum bicrystals (Figure 1) are considered for the study of grain boundary energies. Seventy-nine bicrystalline samples with different types of GBs are investigated; the sizes of each system vary to preserve periodic boundary conditions, but on average they are $30 \times 20 \times 15$ nm^3. The crystallographic directions of the crystal grains before their rotation correspond to the indices [100], [010], [001]. All investigated bicrystals can be divided into 2 types. In the first case, a symmetric rotation of the crystal around the *X* axis corresponding to the [100] direction is performed, and the GB symmetric twist dataset is obtained (yellow arrows in Figure 1). In the second case, the grains are asymmetrically rotated around the Y axis corresponding to the [010] direction, and a set of symmetric and asymmetric tilt GBs is obtained (blue arrows in Figure 1). All the initial bicrystalline systems are created using the ATOMSK software package [38]. The constructed bicrystal sets are maintained at constant temperature and the minimum value of stress tensor components using the Nose–Hoover thermostat and barostat in MD simulations to investigate the effect of temperature on the energy and structure of GBs. MD modelling is performed by the LAMMPS package [39], where the interatomic interaction is described by the ADP potential [40], which is based on the EAM potential [41]. It is worth noting that the GB energies calculated using this EAM potential [41] are in good agreement with both density functional theory (DFT) calculations and MD modelling results using machine learning potentials [29]. The bicrystals are first annealed at high temperature (700 K) to stabilize the boundary structure before the GB energy calculation stage in MD simulations, and then the investigated temperature is set using the Nose–Hoover thermostat. Each investigated system is maintained at constant temperature and minimum stresses for GB energy calculation during 200–300 ps, depending on the temperature considered (200 ps–100 K; 200 ps–300 K; 250 ps–500 K; 300 ps–700 K).

The GB energy is calculated as the excess of the total energy in the bicrystalline system with GB relative to the energy of the system with the same number of atoms and defect-free lattice. The difference between the total energy in the system with GB and the sum of energy per atom in the defect-free crystal is calculated at each simulation step as follows:

$$\gamma_{\mathrm{gb}} = \frac{E_{\mathrm{gb}}(T) - NE_{\mathrm{bulk}}(T)}{2A}, \tag{1}$$

where $E_{\mathrm{gb}}(T)$ is the total energy in the system with GBs at temperature T, $E_{\mathrm{bulk}}(T)$ is the total energy per atom in the ideal crystal at temperature T, N is the number of atoms in the system, and A is the area of the GB. It is duplicated since there are 2 identical boundaries in

the bicrystal due to periodic boundary conditions. According to Equation (1), the energy is calculated every picosecond during the energy calculation stage, and then the average and minimum grain boundary energies are determined from these data. This is done in order to calculate the average energy over the GB ensemble, since even with a fixed grain misorientation, there are many metastable structures with different energies. The size of the bicrystalline system is sufficient to adequately measure the energy of the GBs, which is evident from the comparison of the energy curves obtained in this work with the results of other experimental and numerical studies on the example of symmetric tilt and twist boundaries (Figure 2).

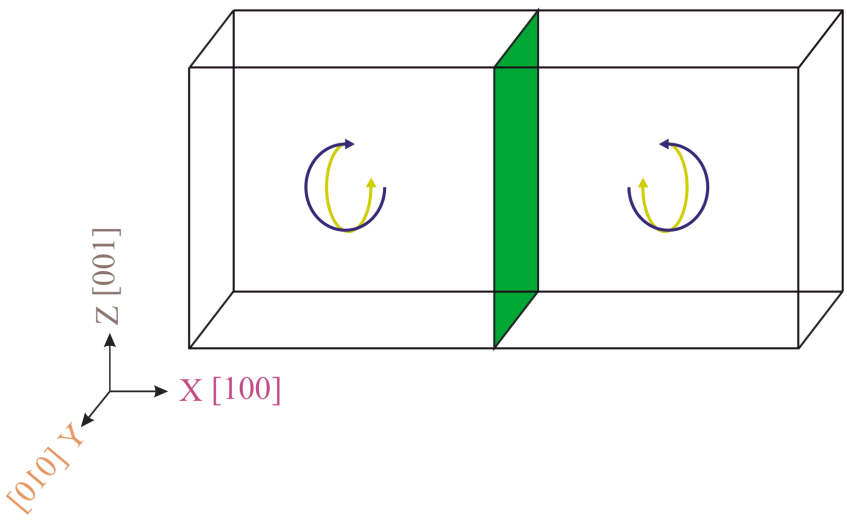

Figure 1. Scheme of bicrystalline grains rotation for obtaining grain boundaries of different types: green color indicates the plane of GB; blue arrows indicate rotation with respect to *Y* axis (tilt boundary); yellow arrows indicate rotation with respect to *X* axis (twist boundary).

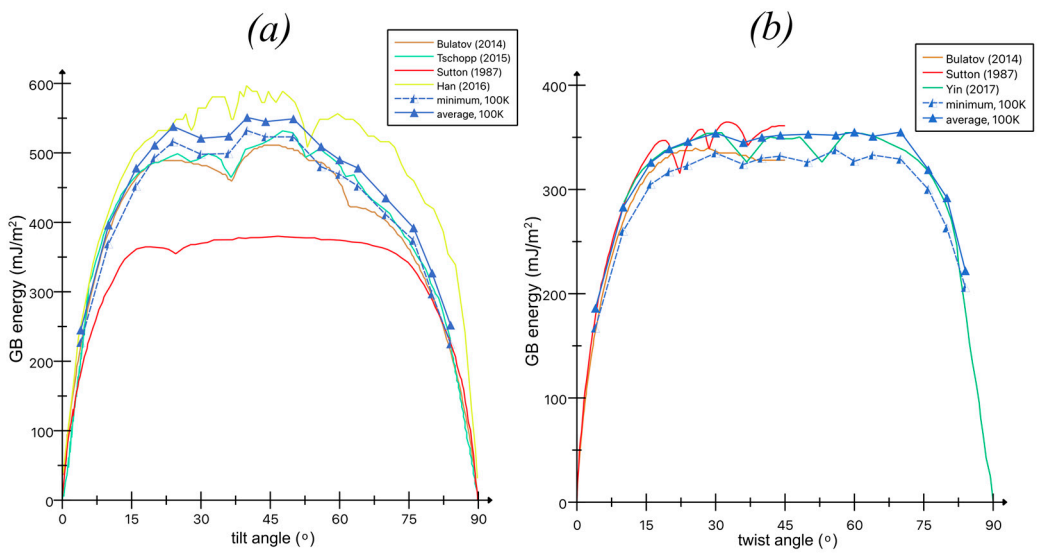

Figure 2. Energy of symmetric tilt (**a**) and twist (**b**) GBs for T = 100 K obtained from MD simulations and their comparison with data from other works: adapted from [25] is interpolation of GB energy data obtained by MS simulations (BRK function); adapted from [21] is GB energies obtained by MS simulations; adapted from [5] is GB energies obtained by MD simulations at 10 K; adapted from [15] is the experimental data on GB energies; adapted from [23] is average GB energies for the ensemble of metastable and stable structures obtained from atomistic simulations.

3. Results

3.1. Influence of Temperature on GB Energy

Let us compare the results of GB energies with existing works on the example of energy curves for symmetric tilt and twist GBs in aluminum with respect to the crystallographic orientation [100] (Figure 2) before presenting them for different temperatures. The reported results from other works can be categorized into 3 types: (i) The minimum GB energy calculated in MD simulations at temperature T = 10 [5] and in MS simulations [21,25], (ii) experimental data on the boundary energies [15] and (iii) average energies of stable and metastable GBs from MD simulations [23]. Figure 2 shows the average and minimum energies from our calculations for the temperature of 100 K for comparison to previously listed data. The average values of the tilt GB energies are compared with the data (iii): Our results for symmetric tilt boundaries (Figure 2a) underestimate the values in (iii), because the number of emerging structures for the GB with fixed grain misorientation at the measurement stage of MD simulations is insufficient compared to considering all possible stable and metastable GB structures in the study [23]. The average energies of this type of boundary are higher than the minimum values in (i) and the experimental data (ii). In contrast to the case of symmetric tilt boundaries, the average energy for symmetric twist GBs (Figure 2b) is within the range of the given data (i) and (ii), because the metastable structures and energy scatter are much lower for this type of GB, which is consistent with the description of these boundaries in work [23]. The minimum values of the GB energy are given for comparison with type (i) data. Our results for symmetric tilt boundaries (Figure 2a) give a slight overestimation, while the results for symmetric twist boundaries (Figure 2b), on the contrary, slightly underestimate the data (i). Nevertheless, our results are in sufficient qualitative and quantitative agreement with the data (i). Experimental data (ii) are given for qualitative evaluation, because, as mentioned above, the experimental data on GB energies even at present are mainly qualitative [18]. All curves shown in Figure 2 obtained from atomistic modelling qualitatively describe data (ii).

To obtain the GB energy at different temperatures, it is necessary to calculate the energy per atom in the defect-free crystal. The values of these energies are given in Table 1. For comparison, data from other works are also found: −3.36 eV/atom for 10 K [5]; −3.288 and −3.283 eV/atom for 300 K [6].

Table 1. Value of energies per atom in the defect-free crystal for temperatures range from 10 to 700 K.

Temperature (K)	Bulk Energy on Atom (eV/Atom)
10	−3.357
100	−3.334
300	−3.283
500	−3.23
700	−3.175

Let us turn to the results for different temperatures. Figure 3 shows the results for the symmetric tilt and twist GBs, including the average (Figure 3b,d) and minimum (Figure 3a,c) energies for temperatures of 100, 300, 500, and 700 K. Let us consider the effect of temperature on symmetric twist GBs (Figure 3a,b). The minimum GB energies generally decrease with increasing temperature, while the average energies increase. For this type of boundary, there are no special boundaries with features in energy (e.g., boundaries of coherent twins with very low energies). The only thing that can be noticed is that the energy spread at low-angle boundaries is smaller than for high-angle boundaries. This may be due to the fact that the low-angle twist boundaries have a rather stable structure, namely, the dislocation grid, which does not change with temperature increase from 10 to 700 K (Figures 4 and 5). The presented structure of twist GB is in agreement with already available studies [42,43]. While general high-angle twist boundaries do not have a strictly defined structure, their energy spread is larger. The average and minimum energy curves for symmetric tilt GBs are shown in Figure 3c,d. In the boundaries of this type,

there are quite a large number of special high-angle GBs within the inclination angles [28]. Therefore, it can be observed that the energy spread for high-angle boundaries is not always large and is comparable or even smaller than for low-angle boundaries (e.g., the range of inclination angles from 50 to 75° for the minimum energy). The average energies increase with increasing temperature, while the minimum energies decrease up to and including temperature of 500 K and can either decrease or increase with further temperature increase. The average energies in both cases (tilt and twist boundaries) grow non-linearly with increasing temperature, which can be observed from the energy difference in the temperature ranges 100–300 K, 300–500 K, and 500–700 K. The difference between the average energies in the latter interval is much larger than in the first two, which is mostly true for high-angle boundaries. If we consider the behavior of the minimum energy in the same temperature intervals, we see a more complex dependence on temperature. The energy can non-linearly decrease (tilt boundaries) at some misorientation angles, and the decrease in the minimum energy can be comparable in some temperature intervals (high-angle twist boundaries) or even go back to the increase (tilt boundaries at 700 K). If we look at the picture of the GB variation from temperature as a whole in Figure 3, we can see a complex non-linear relationship between energy, grain misorientation, and temperature.

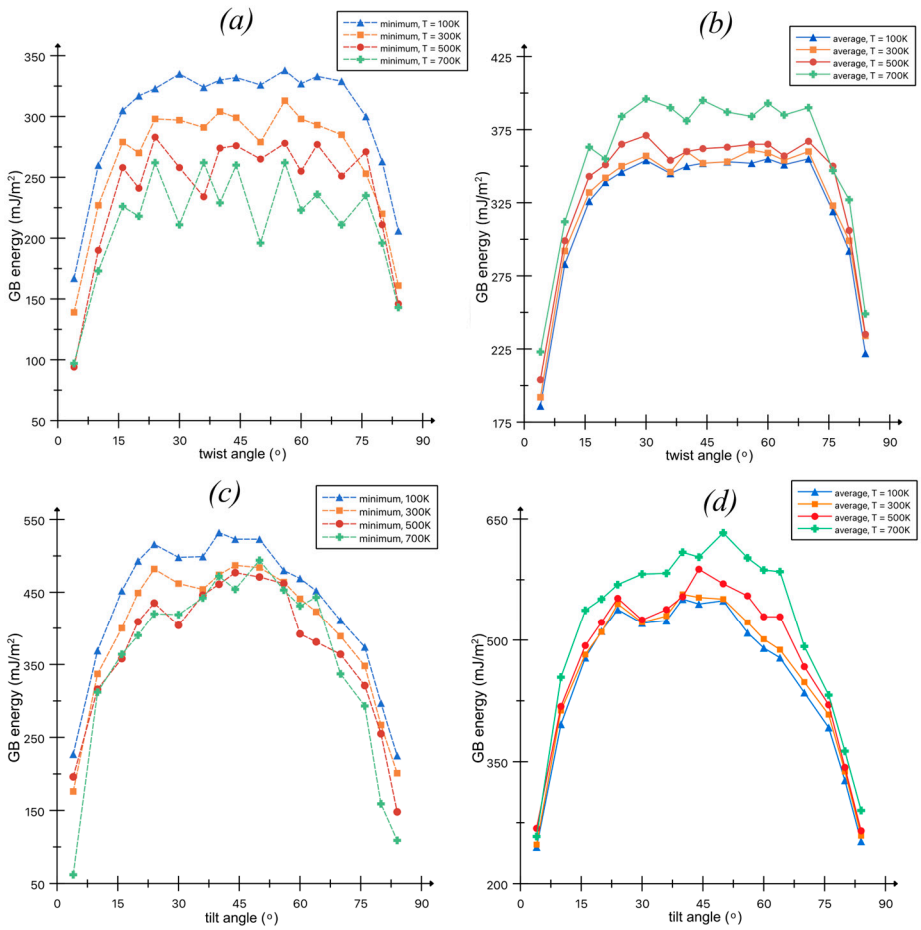

Figure 3. Energy curves of symmetrical twist (**a**,**b**) and tilt (**c**,**d**) GBs in the plane (100) for different temperatures 100, 300, 500 and 700 K: minimum GB energy values obtained in the MD modelling measurement stage for each boundary (**a**,**c**); average GB energy values over all obtained GB energies in the MD modelling measurement stage for each boundary (**b**,**d**).

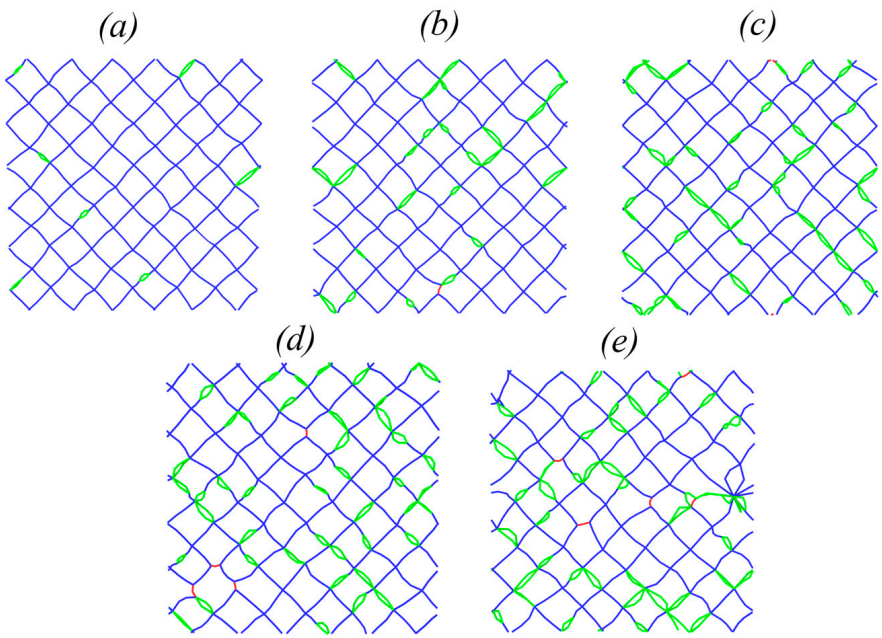

Figure 4. Dislocation structure of the low-angle twist GB [100] with the misorientation angle of 10° at system temperature: (**a**) 10 K, (**b**) 100 K, (**c**) 300 K, (**d**) 500 K, (**e**) 700 K. Blue lines are perfect dislocations, green lines are Shockley dislocations.

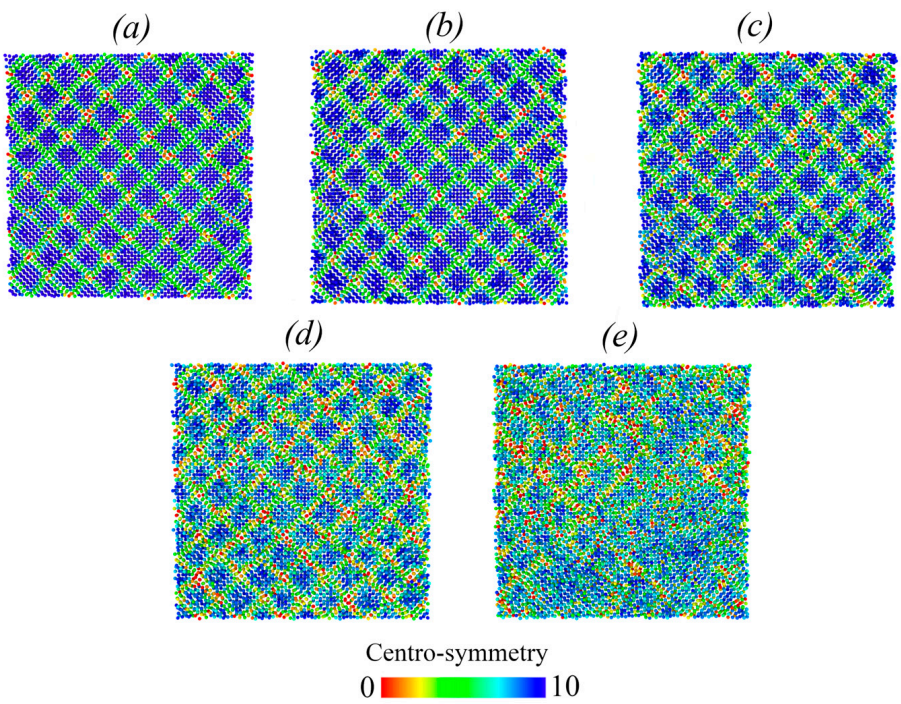

Figure 5. Atomic structure of the low-angle twist GB [100] with the misorientation angle of 10° at the system temperature: (**a**) 10 K, (**b**) 100 K, (**c**) 300 K, (**d**) 500 K, (**e**) 700 K. The atoms are colored according to the value of the centro-symmetry parameter.

From the MD modelling results, the level of GB energy scattering with increasing temperature can be estimated. Figure 6 shows the level of decrease in the minimum energy and the total scatter (taking into account the minimum and average energies) for the temperature range from 100 to 700 K. For this purpose, the scatter of the GB energy with temperature growth is calculated for each grain misorientation relative to the maximum energy difference. As expected for the symmetric twist GBs due to the lack of a

sufficient number of special boundaries, the energy spread (Figure 6c,d) is significant. The largest energy scatter is observed for high-angle boundaries: About a 30% reduction in the minimum energy and about 40% of the total spread. The smaller energy spread is observed for low-angle twist GBs, which is consistent with the above arguments about the greater stability of the structure of such GBs: About a 17% decrease in the minimum energy and about 28% of the total spread. Let us consider the energy spread in the symmetric tilt GBs (Figure 6a,b). The presence of a sufficiently large number of special boundaries leads to the fact that the scatter of the total energy (Figure 6b) is generally smaller and shifted towards low-angle boundaries: About 22% of the total spread is for high-angle boundaries and about 28% for low-angle boundaries. The behavior of the minimum energies of the tilt GBs (Figure 6a) is similar: The decrease in the minimum energy of the high-angle boundaries is about 12%, and that of the low-angle boundaries is about 22%. If we compare the results obtained with the energy reduction in some special boundaries in pure aluminum measured in other works [22,34,44] based on atomistic simulations for different structural units and GBs (the percentage values of grain boundary energy reduction are presented in Table 2), we can see that the results of this work show energy reductions comparable to the data from other work. Table 2 shows the energy change of several types of GBs, where the choice of boundaries is determined according to the Σ values. First, the above studies [22,34,44] consider GBs relative to the crystallographic plane (111) with several values of Σ, where the titles "domino", "pearl", "A" and "C" are internal designations of different structural units that can form boundaries with the considered values of Σ [22]. Second, GBs with respect to the crystallographic plane (110) [34] and (100) [44] were considered in these works. Of all the GBs, only for the Σ5 boundary [44] are the results of energy change with different structures designated by the authors as "type 1" and "type 2" given.

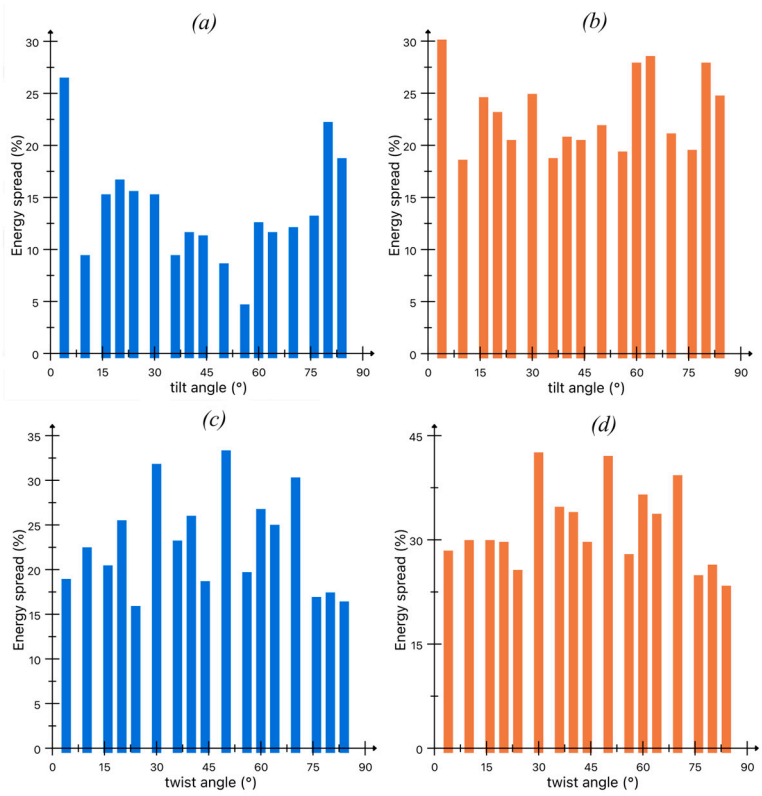

Figure 6. Energy scatter of tilt (**a**,**b**) and twist (**c**,**d**) GB energies in the temperature range from 100 to 700 K obtained in MD simulations: (**a**,**c**) scatter of minimum energies; (**b**,**d**) total scatter of average and minimum energies.

Table 2. Percentage values of energy reduction with increasing temperature for some special GBs obtained in the works, adapted from [22,34,44].

Type of Grain Boundary	Type of Structural Unit	Temperature Range (K)	Energy Reduction (%)
Σ49 [22]	domino	0–600	12.7
	pearl	0–600	14.7
Σ19b [22]	pearl	0–800	28
	domino 1	0–800	22
	domino 2	0–800	26
Σ37c [22]	pearl 1	0–800	20
	pearl 2	0–800	21
	pearl 3	0–800	26
	domino	0–800	20
Σ13b [22]	pearl	0–800	29.5
	domino	0–800	26
	A	0–800	25.1
Σ7 [22]	pearl	0–1000	43.7
	domino	0–1000	23
	C	0–1000	47
Σ5 [44]	type 1	0–400	14.4
	type 2	0–400	6.5
Σ11 [44]	-	0–400	5
Σ9 [34]	-	0–300	10

3.2. Description of the GB Energy Function in the Form of Feed-Forward Neural Network

As discussed above, there is a complex non-linear dependence between the GB energy from temperature and grain misorientation, the form of which is unknown to us. However, this problem can be solved by applying machine learning methods. It is possible to fit such a function that describes the energy of tilt and twist grain boundaries with respect to the crystallographic plane (100) in the form of a fully connected forward propagation neural network. The advantage of using FCNN is that, with a relatively small set of values of the GB energy, this type of functional dependency can predict the GB energy for intermediate temperatures in the continuous range [100, 700] K based on data for the fixed temperatures 100, 300, 500, and 700 K from MD simulations. This is relevant because the calculation of the GB energy is conceptually simple but computationally complex for each boundary.

In this case, the FCNN is a surrogate (or approximation) of the GB energy function in the form $\gamma_{\mathrm{gb}} = f\left(\vec{\Theta}, T\right)$, where the vector $\vec{\Theta} = (\theta_{\mathrm{tilt}}, \theta'_{\mathrm{tilt}}, \theta_{\mathrm{twist}}, \theta'_{\mathrm{twist}})$ contains the rotation angles of both grains. The FCNN scheme is shown in Figure 7. The essence of FCNN is the sequential computation of activation functions (arrows in Figure 7 show the direction of computation), where the input value per neuron of each layer can be computed as:

$$z_i^l = \sum_k w_{ik}^l a_k^{l-1} - b_i^l, \text{ where } l = 1,\ 2, \cdots, L;\ i, k = 1, 2, \cdots, n, \tag{2}$$

where i is the index by neurons in layer l, k is the index by neurons in layer l-1, l is the index by layers of the network, L is the number of layers of the network, and n is the number of neurons in each layer. In Equation (2), the value of the activation function with zero index ${a^0}_i$ is taken as input data, i.e., $\vec{\Theta}, T$. The FCNN output layer calculates the result of the function, in this case γ_{gb}, as described by the sigmoidal activation function:

$$a_i^L = \frac{1}{1 + e^{-(z_i^L)}}. \tag{3}$$

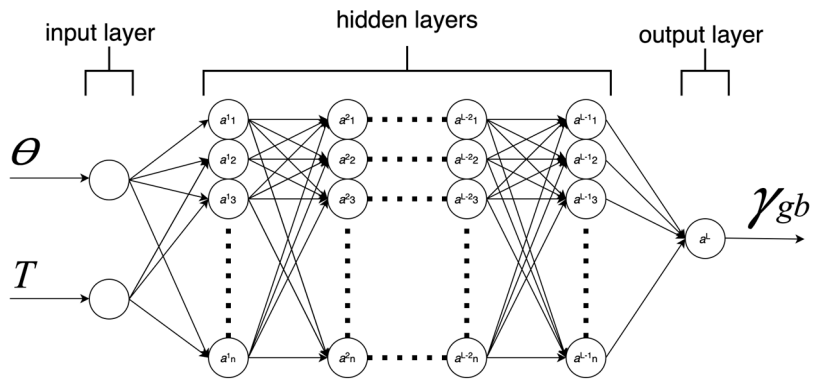

Figure 7. Schematic of the forward propagation neural network, which describes the GB energy (output layer) as a function of the misorientation angle and temperature (input layer).

We considered 2 variants of FCNN in which different activation functions are used to describe the hidden layers. In the first variant of FCNN it is a piecewise linear function PReLU [45]:

$$a_i^l = \begin{cases} \alpha_{\text{prelu}} z_i^l \text{ if } z_i^l < 0 \\ z_i^l \text{ if } z_i^l \geq 0 \end{cases}, \tag{4}$$

where α_{prelu} is the parameter determining the slope of the straight line in the negative region of the PReLU function. In the second variant, the non-linear activation function Swish [46] is used:

$$a_i^l = \frac{z_i^l}{1 + e^{-(\beta z_i^l)}}, \tag{5}$$

where β is the parameter of the Swish activation function determining its non-linearity. Both FCNN variants are trained using the Adam algorithm [47]. Adam is an optimization of a stochastic gradient descent algorithm with a variable learning rate. Three datasets are used to train and check the generalizability of the neural network: Training, validation, and testing. Datasets are compiled from the MD simulation data described in Chapter 3.1, then randomly mixed and distributed into specific sets, the proportion of which is determined by the set of hyperparameters. The main hyperparameters of the learned FCNNs, the hyperparameters associated with the training algorithm, and the distribution and size of the datasets used for training, validation, and testing are presented in Table 3. Hyperparameters such as network depth, number of neurons per layer, and value of activation function parameters (α_{prelu} and β) are selected by repeatedly running the FNCC training with different values of these parameters. Table 3 summarizes the optimal parameters at which the FCNN is trained with maximum accuracy. In the first iteration of training, the initial Adam step is set as standard (0.001). At the additional iteration of training, i.e., when FCNN was pre-trained with the parameter values from the initial training, the value of the initial step is chosen 10 times smaller so that the increments of FCNN parameters are minimal. The number of training epochs is chosen according to the "Early stopping" strategy: Every 10 training epochs, a cross-validation procedure is performed, and the FCNN parameter values with the lowest generalization error are stored. The cross-validation technique involves calculating the average and maximum error on the training and validation sets in the process of FCNN training. The smallest generalization error is estimated as the maximum accuracy on validation and training data in the aggregate, with the smallest gap between accuracy on training and validation data, which avoids overtraining of the FCNN. Table 3 shows the epochs at which the network configuration is stored.

Table 3. Main hyperparameters of the learned FCNNs.

Parameters	FCNN 1 (PReLU Activation)	FCNN 2 (Swish Activation)
α_{prelu}, β (PReLU or Swish parameter)	4.0	0.1
Number of hidden layers, l	8	6
Number of neurons per hidden layer, n	15	15
μ (initial Adam step)	0.001	0.001 (pre-training); 0.0001
Number of epochs	6435	7335 (pre-training); 45
Amount of training data (samples)	610 (82.5%)	
Amount of validation data (samples)	71 (10%)	
Amount of testing data (samples)	35 (7.5%)	

To determine the accuracy of FCNN, mean absolute percentage errors (MAPE) for all datasets are calculated. As described above, errors on training and validation data are calculated during the training process, and the FCNN configuration with the least generalization error is preserved. To check the network accuracy on new data that is not used in training or cross-validation processes, the resulting FCNN configuration is used on the test dataset, and errors are calculated. The obtained error values are presented in Table 4. To clarify the accuracy of the trained FCNNs, the mean and maximum relative errors are calculated on all datasets. The mean errors show the accuracy of the FCNN as a whole, while the maximum error indicates possible local spikes that can be observed in the correlation curves (Figure 8). If there are no strong deviations in accuracy on the training data, spikes for some points can be observed for the validation and test datasets. However, it should be taken into account that the total number of points in the datasets is small and the energy intervals between points from MD data are quite large (Figure 3). Therefore, the obtained accuracy spikes are within reasonable limits and can be corrected by adding new energy points for new GBs with other grain misorientations. Correlation curves are presented only for the second FCNN variant because, as will be shown later, the use of Swish activation functions leads to more physically reasonable results. In addition, smaller mean errors are observed for the second FCNN variant compared to the first FNCC variant, but slightly more peaks are observed in the validation data (Table 4, Figure 8).

Table 4. Accuracy of the two FCNN variants on all datasets.

Type of Dataset	Error Type	FCNN 1 (PReLU Activation), MAPE (%)	FCNN 2 (Swish Activation), MAPE (%)
Training	Average	0.54	0.41
	Maximum	6.43	6.24
Validation	Average	1.49	1.43
	Maximum	8.67	13
Test	Average	1.51	1.07
	Maximum	13.23	13.56

Trained FNCCs are run at fixed input temperatures of 100, 300, 500, and 700 K and at misorientation angles from 0 to 90° in 1° steps to compare FCNN predictions and MD simulation results. The comparisons are performed for symmetric tilt (Figure 9) and twist (Figure 10) GBs. Both variants of FCNN are considered. It can be seen that for symmetric tilt GBs, the second variant of the network (Figure 9a) describes the energy function of grain boundaries in a continuous range of angles much better and shows features of the GB energy curve where they should be compared to data from other works (Figure 2a).

The use of piecewise linear functions in the hidden layers (the first variant of FCNN) results in the neural network poorly interpolating the point-to-point intervals from the MD calculations (Figure 9b). Let us move on to the symmetrical twist GBs case (Figure 10). Here again, the use of the Swish function gives a more adequate approximation of the energy function. However, both FCNNs have features on the energy plots (at 100 K) and give erroneous values with increasing temperature for the twist boundaries. Significant errors on all datasets occur for this type of grain boundary, which can only be solved by increasing the dataset with new energy points from MD simulations.

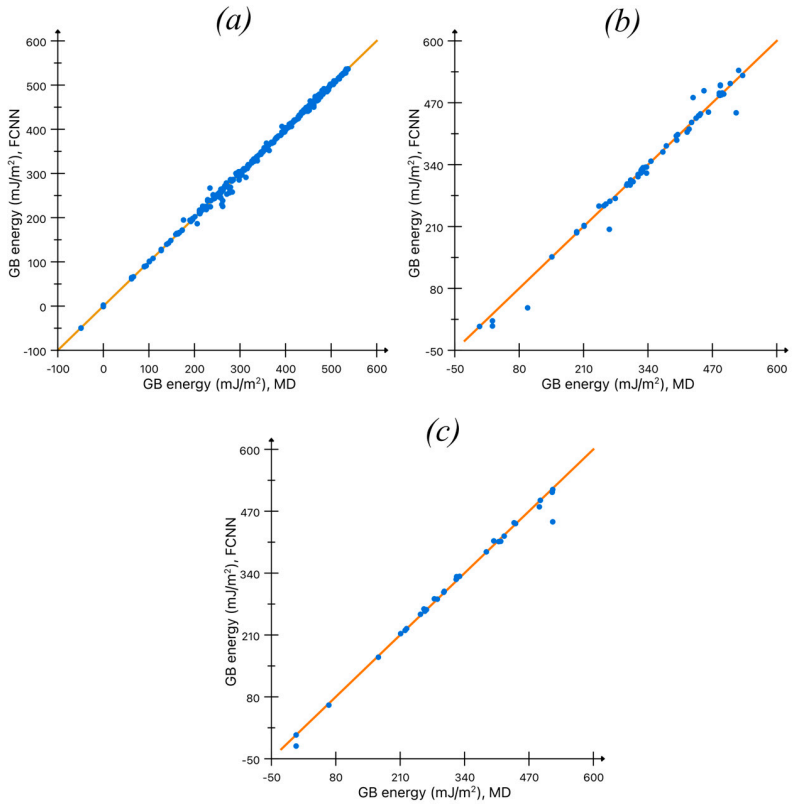

Figure 8. Correlation curves for the second variant FCNN with Swish activation function in the hidden layers: (**a**) Training dataset; (**b**) validation dataset; (**c**) test dataset. The yellow line in the graph shows the ideal accuracy and the blue dots the real accuracy of the learned FCNNs compared to data.

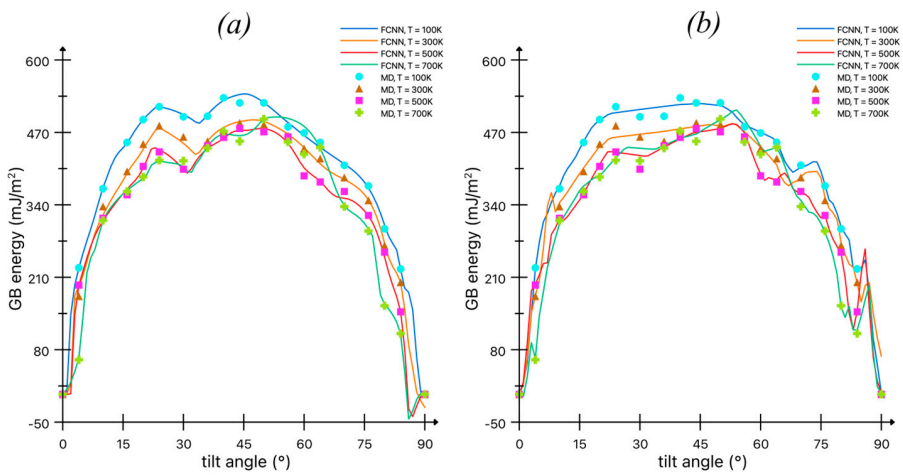

Figure 9. Comparison of the predictions of two FCNN architectures on the example of symmetric tilt GBs: with Swish activation functions in hidden layers (**a**), with PReLU activation function in hidden layers (**b**).

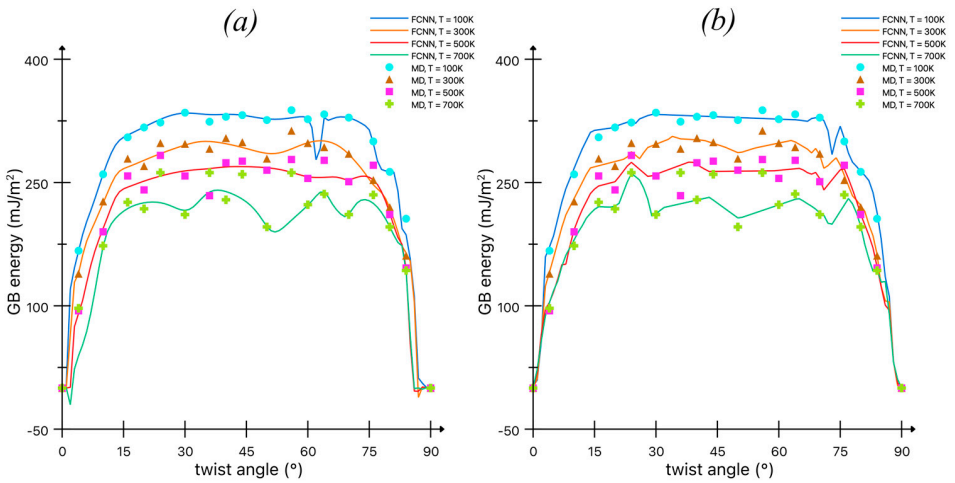

Figure 10. Comparison of the predictions of two FCNN architectures on the example of symmetric twist GBs: with Swish activation functions in hidden layers (**a**), with PReLU activation function in hidden layers (**b**).

To demonstrate the ability of the second version of FNCC to adequately reproduce the energies of GBs for intermediate temperatures not available in the datasets, the FCNN predictions of the minimum energies of the tilt and twist boundaries for temperatures of 200, 400, and 600 K are shown (Figure 11). In the case of tilt GBs (Figure 11a), the energy curves at intermediate temperatures show the same energy distribution pattern (similar curve shape), and the decrease in the minimum energy with increasing temperature is consistent with the general trend of the data. In the case of twist GBs (Figure 11b), a general trend of decreasing GB energy with increasing temperature is also observed for intermediate temperatures.

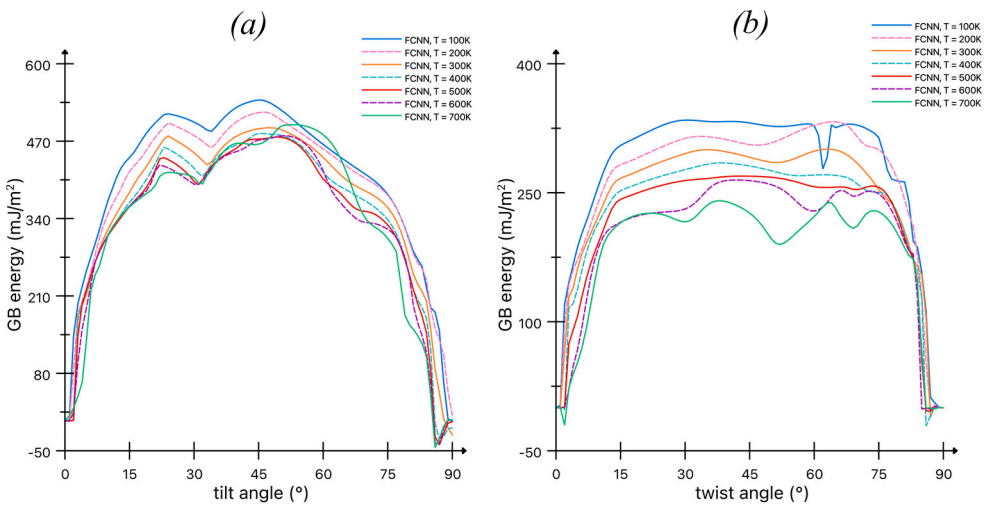

Figure 11. Results of the second variant of FCNN for temperature values missing in the datasets, namely 200, 400, and 600 K. Straight lines are curves for temperatures from the datasets, dashed lines are curves for temperatures missing in the datasets: (**a**) tilt GBs, (**b**) twist GBs.

4. Discussion

This work shows the variation in the GB energy with increasing temperature for the tilt and twist grain boundaries in aluminum, both for low-angle and high-angle types. The variation of the GB energy has been investigated in other works [6,22,23,35,44], where it is shown that even the boundary with a fixed misorientation can have the energy in a wide range of values. However, these studies consider the relationship between the energy

of the boundary and its stable and metastable configurations. In this paper, the energy variation associated with the temperature change of the material is investigated. We show a change in the minimum boundary energies: There is a decrease in energies with increasing temperature by about 20% (Figure 6a,c), which is in agreement with measurements from other works (Table 2). However, we additionally present a change in the average GB energy obtained in the MD simulation stage of measurement GB energy (Figure 6b,d): The increase in energy with increasing temperature is observed. This result is novel and has not been reported in other studies. The energy change shows that many metastable boundaries have energies much higher than in stable configurations, and the occurrence of metastable configurations is due to the motion of atoms at the boundary area [6,23]. Then the appearance of metastable boundary configurations may be the reason for the increase in the average GB energy with increasing temperature. Let us consider the structure of the low-angle twist GB (Figures 4 and 5) with a misorientation angle of 10° as a case of the stable GB structure, in which there is also a significant change in energy with an increase in temperature. It can be seen that the dislocation structure does not actually change with the temperature increase (Figure 4). There are local splits of full dislocations into two partial Shockley dislocations. But this is a typical dislocation reaction in FCC metals [42], which occurs because it is more energetically beneficial. On the other hand, one can see the movement of atoms on the GB plane, considering the atomistic structure of this boundary (Figure 5). Atoms on the boundary are colored according to the value of the centro-symmetry parameter in the FCC lattice, and it can be seen that as the temperature increases, the atoms begin to move in the boundary plane, and the initial characteristic structure of the boundary is lost (Figure 5d,e). This is in agreement with the above-mentioned feature that the change in energy of the grain boundaries is associated with the movement of atoms in them.

As is known, the mobility of the GB is proportional to the boundary energy [2,12,33], so the data obtained in this work can be used to study and simulate the movement of the GB, taking into account changes in the temperature of the material. In turn, the movement of GB makes a significant contribution to the processes of recrystallization and changes in the grain structure [1,3,12]. As work on the study of boundary motion shows, data on boundary energies can be used in tabular [33] or functional form [1–3,12]. Obviously, functional dependence is more acceptable, if only because it allows one to predict energy values in a continuous range of misorientations [24,25]. In this work, we use artificial neural networks to implement functional dependence. We obtained a continuous dependence of the GB energy on misorientation and temperature in the form of the feed-forward fully connected ANN. At the same time, we selected an accurate neural network architecture that can adequately predict boundary energies with intermediate values of temperature and misorientation (Figure 11). This architecture uses non-linear Swish activation functions. In future work, we plan to apply the obtained functions in the form of the ANN to simulate the movement of grain boundaries and eliminate the influence of temperature on this process.

5. Conclusions

On the basis of atomistic simulation data of bicrystalline systems with different grain misorientation angles, we measured the energies of tilt and twist GBs relative to the crystallographic plane (100) for different system temperatures of 100, 300, 500, and 700 K. The average and minimum energies of tilt and twist GBs are calculated, and the main behavior of the obtained energies with increasing temperature is described. The scatter of GB energies in the temperature range of 100 to 700 K is obtained. The feed-forward neural network as a function of GB energy from temperature and grain misorientation is trained on the basis of MD simulation data on GB energies.

1. As the results show, the average energies calculated from all obtained energy states of the GB with fixed grain misorientation at the MD modelling stage of maintaining the bicrystalline system at constant temperature and minimum stress growth with increasing temperature. At the same time, the minimum energies obtained at this MD

stage decrease with increasing temperature, which is in agreement with the results of other studies. Both direct measurements of the GB energy based on atomistic modelling and measurements of the relative GB energy based on experiment.

2. The obtained energy spread shows the level of decrease in the minimum GB energy with increasing temperature and the level of total energy change with taking into account the increase in the average energy of the boundaries. It is shown that the energy spread is generally larger for the twist GBs, with the maximum energy growth observed in the region of high-angle boundaries. The level of energy change with increasing temperature is smaller for the tilt GBs; the energy spread shifts towards low-angle boundaries, which may be due to a rather large number of special high-angle boundaries. The decrease in the minimum energy is compared with the results of other works and is in reasonable agreement, and the average energy decrease is about 20%.
3. Using the example of a trained FCNN with non-linear Swish activation functions in hidden layers, it is shown that the prediction of GB energies using this FCNN is more physically reasonable. Such a network reproduces more adequate point-to-point interpolation of GB energies obtained from MD simulations, which is particularly strong for tilt boundaries. The trained FCNN is able to describe GB energies for intermediate temperatures in a continuous range from 100 to 700 K, as shown for several temperatures missing in the dataset: 200, 400, and 600 K.

Funding: This research and the APC were funded by the Russian Science Foundation, grant number 22-71-00090, https://rscf.ru/en/project/22-71-00090/.

Data Availability Statement: The data presented in this study are available on request from the corresponding author due to the most essential data of MD simulations are presented in graphical form in the article, the coefficients of FCNNs and other data are available upon request.

Conflicts of Interest: The author declares no conflicts of interest.

References

1. Salama, H.; Kundin, J.; Shchyglo, O.; Mohles, V.; Marquardt, K.; Steinbach, I. Role of inclination dependence of grain boundary energy on the microstructure evolution during grain growth. *Acta Mater.* **2020**, *188*, 641–651. [CrossRef]
2. Hallberg, H.; Bulatov, V.V. Modeling of grain growth under fully anisotropic grain boundary energy. *Model. Simul. Mater. Sci. Eng.* **2019**, *27*, 045002. [CrossRef]
3. Liu, G.; Zhang, D.; Yao, C. Investigation of the grain refinement mechanism in machining Ti-6Al-4V: Experiments and simulations. *J. Manuf. Process.* **2023**, *94*, 479–496. [CrossRef]
4. Wang, K.; Xu, Y.; Zhan, W.; Xu, J. The impact of structural units on the dislocation nucleation of bi-crystal copper grain boundary. *Comput. Mater. Sci.* **2023**, *218*, 111900. [CrossRef]
5. Yin, Q.; Wang, Z.; Mishra, R.; Xia, Z. Atomic simulations of twist grain boundary structures and deformation behaviors in aluminum. *AIP Adv.* **2017**, *7*, 015040. [CrossRef]
6. Burbery, N.J.; Das, R.; Ferguson, W.G. Modelling with variable atomic structure: Dislocation nucleation from symmetric tilt grain boundaries in aluminium. *Comput. Mater. Sci.* **2015**, *101*, 16–28. [CrossRef]
7. Burbery, N.J.; Das, R.; Ferguson, W.G. Thermo-kinetic mechanisms for grain boundary structure multiplicity, thermal instability and defect interactions. *Mater. Chem. Phys.* **2016**, *179*, 254–265. [CrossRef]
8. Zhang, L.; Lu, C.; Tieu, K. A review on atomistic simulation of grain boundary behaviors in face-centered cubic metals. *Comput. Mater. Sci.* **2016**, *118*, 180–191. [CrossRef]
9. Lee, J.-L.; Wang, P.-T.; Lo, K.-C.; Shen, P.-K.; Tsou, N.-T.; Kakehi, K.; Murakami, H.; Tsai, C.-W.; Gorsse, S.; Yeh, A.-C. Effect of serrated grain boundary on tensile and creep properties of a precipitation strengthened high entropy alloy. *Sci. Technol. Adv. Mater.* **2023**, *24*, 2158043. [CrossRef]
10. Li, X.; Guan, X.; Jia, Z.; Chen, P.; Fan, C.; Shi, F. Twin-Related Grain Boundary Engineering and Its Influence on Mechanical Properties of Face-Centered Cubic Metals: A Review. *Metals* **2023**, *13*, 155. [CrossRef]
11. Dolzhenko, P.; Tikhonova, M.; Odnobokova, M.; Kaibyshev, R.; Belyakov, A. On Grain Boundary Engineering for a 316L Austenitic Stainless Steel. *Metals* **2022**, *12*, 2185. [CrossRef]
12. Niño, J.D.; Johnson, O.K. Influence of grain boundary energy anisotropy on the evolution of grain boundary network structure during 3D anisotropic grain growth. *Comput. Mater. Sci.* **2023**, *217*, 111879. [CrossRef]
13. Holm, E.A.; Rohrer, G.S.; Foiles, S.M.; Rollett, A.D.; Miller, H.M.; Olmsted, D.L. Validating computed grain boundary energies in fcc metals using the grain boundary character distribution. *Acta Mater.* **2011**, *59*, 5250–5256. [CrossRef]

14. Ratanaphan, S.; Raabe, D.; Sarochawikasit, R.; Olmsted, D.L.; Rohrer, G.S.; Tu, K.N. Grain boundary character distribution in electroplated nanotwinned copper. *J. Mater. Sci.* **2017**, *52*, 4070–4085. [CrossRef]
15. Sutton, A.P.; Balluffi, R.W. Overview no. 61 On geometric criteria for low interfacial energy. *Acta Metall.* **1987**, *35*, 2177–2201. [CrossRef]
16. Hasson, G.C.; Goux, C. Interfacial energies of tilt boundaries in aluminium. Experimental and theoretical determination. *Scr. Metall.* **1971**, *5*, 889–894. [CrossRef]
17. Li, C.; Lu, S.; Vitos, L. Predicting grain boundary energies of complex alloys from ab initio calculations. *Scr. Mater.* **2021**, *203*, 114118. [CrossRef]
18. Ratanaphan, S.; Sarochawikasit, R.; Kumanuvong, N.; Hayakawa, S.; Beladi, H.; Rohrer, G.S.; Okita, T. Atomistic simulations of grain boundary energies in austenitic steel. *J. Mater. Sci.* **2019**, *54*, 5570–5583. [CrossRef]
19. Kim, H.-K.; Ko, W.-S.; Lee, H.-J.; Kim, S.G.; Lee, B.-J. An identification scheme of grain boundaries and construction of a grain boundary energy database. *Scr. Mater.* **2011**, *64*, 1152–1155. [CrossRef]
20. Holm, E.A.; Olmsted, D.L.; Foiles, S.M. Comparing grain boundary energies in face-centered cubic metals: Al, Au, Cu and Ni. *Scr. Mater.* **2010**, *63*, 905–908. [CrossRef]
21. Tschopp, M.A.; Coleman, S.P.; McDowell, D.L. Symmetric and asymmetric tilt grain boundary structure and energy in Cu and Al (and transferability to other fcc metals). *Integr. Mater. Manuf. Innov.* **2015**, *4*, 176–189. [CrossRef]
22. Brink, T.; Langenohl, L.; Bishara, H.; Dehm, G. Universality of grain boundary phases in fcc metals: Case study on high-angle [111] symmetric tilt grain boundaries. *Phys. Rev. B* **2023**, *107*, 054103. [CrossRef]
23. Han, J.; Vitek, V.; Srolovitz, D.J. Grain-boundary metastability and its statistical properties. *Acta Mater.* **2016**, *104*, 259–273. [CrossRef]
24. Sarochawikasit, R.; Wang, C.; Kumam, P.; Beladi, H.; Okita, T.; Rohrer, G.S.; Ratanaphan, S. Grain boundary energy function for α iron. *Materialia* **2021**, *19*, 101186. [CrossRef]
25. Bulatov, V.V.; Reed, R.W.; Kumar, M. Grain boundary energy function for fcc metals. *Acta Mater.* **2014**, *65*, 161–175. [CrossRef]
26. Zheng, H.; Li, X.-G.; Tran, R.; Chen, C.; Horton, M.; Winston, D.; Persson, K.A.; Ong, S.P. Grain Boundary Properties of Elemental Metals. *Acta Mater.* **2020**, *186*, 40–49. [CrossRef]
27. Ye, W.; Zheng, H.; Chen, C.; Ong, S.P. A Universal Machine Learning Model for Elemental Grain Boundary Energies. *Scr. Mater.* **2022**, *218*, 114803. [CrossRef]
28. Kiyohara, S.; Oda, H.; Miyata, T.; Mizoguchi, T. Prediction of interface structures and energies via virtual screening. *Sci. Adv.* **2016**, *2*, e1600746. [CrossRef]
29. Nishiyama, T.; Seko, A.; Tanaka, I. Application of machine learning potentials to predict grain boundary properties in fcc elemental metals. *Phys. Rev. Mater.* **2020**, *4*, 123607. [CrossRef]
30. Borges, Y.; Huber, L.; Zapolsky, H.; Patte, R.; Demange, G. Insights from symmetry: Improving machine-learned models for grain boundary segregation. *Comput. Mater. Sci.* **2024**, *22*, 034004. [CrossRef]
31. Huber, L.; Hadian, R.; Grabowski, B.; Neugebauer, J. A machine learning approach to model solute grain boundary segregation. *Npj Comput. Mater.* **2018**, *4*, 64. [CrossRef]
32. Feng, B.; Wei, J.; Shibata, N.; Ikuhara, Y. Atomistic grain boundary migration in Al_2O_3. *Int. J. Ceram. Eng. Sci.* **2023**, *5*, e10169. [CrossRef]
33. Kim, H.-K.; Kim, S.G.; Dong, W.; Steinbach, I.; Lee, B.-J. Phase-field modeling for 3D grain growth based on a grain boundary energy database. *Model. Simul. Mater. Sci. Eng.* **2014**, *232*, 112663. [CrossRef]
34. Tucker, G.J.; McDowell, D.L. Non-equilibrium grain boundary structure and inelastic deformation using atomistic simulations. *Int. J. Plast.* **2011**, *27*, 841–857. [CrossRef]
35. Burbery, N.J.; Das, R.; Ferguson, W.G. Transitional grain boundary structures and the influence on thermal, mechanical and energy properties from molecular dynamics simulations. *Acta Mater.* **2016**, *108*, 355–366. [CrossRef]
36. Kelly, M.N.; Bojarski, S.A.; Rohrer, G.S. The Temperature Dependence of the Relative Grain-Boundary Energy of Yttria-doped Alumina. *J. Am. Ceram. Soc.* **2017**, *100*, 783–791. [CrossRef]
37. Foiles, S.M. Temperature dependence of grain boundary free energy and elastic constants. *Scr. Mater.* **2010**, *62*, 231–234. [CrossRef]
38. Hirel, P. Atomsk: A tool for manipulating and converting atomic data files. *Comput. Phys. Commun.* **2015**, *197*, 212–219. [CrossRef]
39. Plimpton, S. Fast Parallel Algorithms for Short-Range Molecular Dynamics. *J. Comput. Phys.* **1995**, *117*, 1–19. [CrossRef]
40. Apostol, F.; Mishin, Y. Interatomic potential for the Al-Cu system. *Phys. Rev. B* **2011**, *83*, 054116. [CrossRef]
41. Mishin, Y.; Farkas, D.; Mehl, M.J.; Papaconstantopoulos, D.A. Interatomic potentials for monoatomic metals from experimental data and ab initio calculations. *Phys. Rev. B* **1999**, *59*, 3393. [CrossRef]
42. Hirth, J.; Lothe, J. *Theory of Dislocations*, 2nd ed.; Wiley: New York, NY, USA, 1982.
43. Zhang, L.; Gu, Y.; Xiang, Y. Energy of low angle grain boundaries based on continuum dislocation structure. *Acta Mater.* **2017**, *126*, 11–24. [CrossRef]
44. Hashimoto, M.; Ishida, Y.; Yamamoto, R.; Doyama, M. Thermodynamic properties of coincidence boundaries in aluminum. *Acta Metall.* **1981**, *29*, 617–626. [CrossRef]
45. He, K.; Zhang, X.; Ren, S.; Sun, J. Delving deep into rectifiers: Surpassing human-level performance on imagenet classification. In Proceedings of the 2015 IEEE International Conference on Computer Vision, Santiago, Chile, 7–13 December 2015; pp. 1026–1034.

46. Ramachandran, P.; Zoph, B.; Le, Q.V. Searching for Activation Functions. *arXiv* **2017**, arXiv:1710.05941.
47. Kingma, D.P.; Ba, J. Adam: A method for stochastic optimization. *arXiv* **2017**, arXiv:1412.6980.